Centrifugal spinning and characterization of CO_3O_4 coated carbon fibers

J. Ayala [a], D. Ramirez [b], E. Fletes [a], H. Morales [b], J.G. Parsons [b,*], M. Alcoutlabi [a,*]

[a] Department of Mechanical Engineering, University of Texas, Rio Grande Valley, 1201 W University Dr. Edinburg, TX 78539, USA
[b] Department of Chemistry, University of Texas, Rio Grande Valley, 1 W University Blvd. Brownsville, TX 78521, USA

ARTICLE INFO

ABSTRACT

Centrifugally spun polyacrylonitrile (PAN) microfibers surface-coated with Co_3O_4 nanoparticles (NPs) were prepared as precursors to produce coated Co_3O_4 carbon-composite fibers. The Co_3O_4/C composite fibers were obtained through a staged heating process during which the Co_3O_4PAN precursor fibers were stabilized over four hours at 200 °C, and subsequently the stabilized fibers were carbonized for six hours at 600 °C. The synthesis process presented in this work provides an effective strategy for the fabrication of surface coated-fiber materials, including composite fibers with good structure and morphology. The characterization of the Co_3O_4/C composite fibers was performed using SEM, EDS, XPS, XRD and BET. The SEM data indicated the fibers were micron-sized in diameter with a non-homogenous distribution of the Co_3O_4 NPs on both the Co_3O_4-PAN and the CO_3O_4-Carbon composite fibers. The EDS mapping of the cobalt showed it to be distributed throughout the samples on the surface, but areas of high concentrations of particles were observed. The powder XRD data showed a reduction of the Co(III)/Co(II) starting material into a combination of Co-metal and CoO. The XRD results were confirmed by the Co 2P XPS data, which showed a change from the pure Co_3O_4 NPs to a combination of Co(III), Co(II) and Co-metal. In addition, the binding of the Co_3O_4 nanoparticles to the PAN fibers before carbonization showed a change in the chemical environment, which included attachment through an N ligand on the fibers.

© 2021 Published by Elsevier B.V.

1. Introduction

Composite nanomaterials and nanofibers have attracted attention in recent years for numerous applications, such as filtration, energy storage, water splitting, tissue engineering, biomedical and catalysis [1–13]. Electrospinning has been the most widely used method to prepare composite-fiber precursors due to its low cost, ease of use and flexibility. However, electrospinning is a time-consuming production process and faces safety concerns due to the required high voltage and high current during fiber formation, especially for melt electrospinning where a high current is needed. Centrifugal spinning has emerged recently as a potential method for its high production rate of fibers and microfibers for a wide range of applications, including filtration, biomedical, tissue engineering and energy storage [4–13].

Fiber formation by centrifugal spinning requires higher viscosity solutions compared to those prepared by electrospinning due to the large centrifugal forces encountered at the high spinneret rotational speeds. The advantage of using centrifugal spinning

is a higher fiber yield compared to that of electrospinning. The centrifugal spinning of precursor fibers with active materials (e.g. ceramic/metallic NPs) becomes difficult with increased NP loading in the precursor solution. These challenges are because the polymer/metal-oxide precursor solutions usually exhibit high viscosity and surface tension, and differing densities, which can affect the ability to produce centrifugally spun fibers at large production scale with the desired structure and morphology. For this reason, recent efforts have been made to find a scalable means for the fabrication of carbon/metal composite fibers [11].

In this work, we report the use of PAN fibers as structural hosts for cobalt (II,III) oxide Co_3O_4 in a successful wet coating-method, which has been used to increase material loading in the carbon-fiber matrix. The characterization of Co_3O_4 composite coated fibers was performed by SEM, EDS, XPS, XRD and BET. In the present work, results on the synthesis, characterization and formation of coated composite fibers prepared from Co_3O_4/PAN precursor fibers are reported. The results show the presence of nitrogen and carbon in the polymer led to the reduction of the Co_3O_4 nanoparticles in the composite processing stage. While similar works have been performed to improve the electrochemical performance of carbon fibers using iron-oxide coated carbon fibers as electrodes in lithium ion batteries, the purpose of the

* Corresponding authors.
E-mail addresses: jason.parsons@utrgv.edu (J.G. Parsons), mataz.alcoutlabi@utrgv.edu (M. Alcoutlabi).

present study was to develop a method of increased surface coating dispersion and to understand the adsorption mechanisms as a model to enable the development of future carbon/metal-oxide composite-fibers for several applications.

2. Experimental

2.1. Materials

Polyacrylonitrile (PAN) (average M of 150,000 g/mol), dimethylformamide (DMF) 99.5%, ethanol 9.5% and cobalt oxide nano powder (Co_3O_4, 99%, 10–30 nm) were purchased from Sigma Aldrich. Ethylene carbonate (EC) (99%) and dimethyl carbonate (DMC) were purchased from Alpha Aesar and Fisher Scientific, respectively.

2.2. Carbon fiber preparation

Polymer precursor solutions were prepared at a concentration of 12 wt. % PAN in DMF and subsequently stirred for 24 h using mechanical stirring to obtain homogeneous mixtures. The pristine PAN microfibers were obtained through centrifugal spinning at rotational speeds ranging from 6500 to 8000 rpm, with a relative humidity below 40%. The fibers were collected using a rectangular aluminum substrate and dried under vacuum at 60 °C. The stabilization of the PAN microfibers was performed by heat treatment, which consisted of heating the PAN mats in an OTF-1200X tube furnace (MTI Corp. California, USA) in air at 280 °C for 4 h (heating at a rate of 3 °C/min). The PAN microfibers were carbonization in an argon atmosphere at 600 °C for 6 h. Fig. 1 shows a schematic of the composite-fiber preparation by centrifugal spinning and subsequent heat treatment

2.3. Preparation of coated carbon fibers

The Co_3O_4 coated carbon fibers were prepared by diluting the Co_3O_4 nano-powder into ethanol and stirring for 5 h. After stirring, the mixture was sonicated for 1 h. Fibrous mats were placed flat on a glass surface and dipped into the ethanolic suspension of Co_3O_4 nanoparticles and sonicated for 1 h. The PAN fibrous mats were weighed and coated with either 30 or 70 wt% of Co_3O_4 nanoparticles. The samples were then allowed to soak for 24 h and placed in an OTF-1200X tube furnace, stabilized under air at 280 °C for 4 h (heating at a rate of 3 °C/min) and carbonized under an argon atmosphere at 600 °C for 6 h.

2.4. Characterization

The composite fibers were characterized before and after carbonization using X-ray diffraction (XRD). The diffraction patterns were collected in 2Θ from 10–80°, with a step of 0.05, a 5 s counting time, a Co source (Co $K_\alpha = 1.789$ Å) and with a nickel filter on a Bruker D2 X-ray diffractometer. Scanning electron microscopy (SEM) imaging and EDS were collected using a Sigma VP Carl Zeiss Scanning electron microscope with an attached EDAX (Octane Super) detector. X-ray photoelectron spectroscopy (XPS) data was collected using a Thermo Scientific K-Alpha X-ray photoelectron spectrometer to characterize the surface composition of the Co_3O_4 coated carbon fibers. Surface area (BET) experiments of the composite fibers were performed using a Nova 2200e surface area and porosity analyzer (Quantachrome Instruments).

Table 1
EDS results on Co_3O_4/PAN composite fibers for carbon, nitrogen, cobalt, and oxygen concentrations.

Element	at % Area 1	wt% Area 1	at % Area 2	wt% Area 2	at % Area 3	wt % Area 3
C	66.91	53.94	56.22	42.66	84.03	78.88
N	14.60	13.73	15.60	13.81	13.93	15.25
O	14.15	15.19	22.63	22.88	1.050	1.313
Co	4.33	17.13	5.542	20.64	0.99	4.56

3. Results and discussion

3.1. Surface morphology and characterization. SEM analysis

Fig. 2A shows the reaction product between the PAN fibers and the Co_3O_4 nanoparticles. As can be observed, the Co_3O_4 NPs appear to be aggregated in small areas on the surface of the PAN fibers and the figure indicates that the distribution of Co_3O_4 on the surface is not homogenous. At a higher magnification, as shown in Fig. 2B, the data confirms the aggregation of the Co_3O_4 particles at/on the surface of the fibers. Both Fig. 2A and B show the typical fiber surface morphology of PAN fibers prepared by centrifugal spinning. The fibers are homogeneous with respect to diameter and do not show evidence of excess solvent during the spinning process. The presence of excess solvent is typically denoted by the formation of nodules in the fibers [12]. In addition, the surface of the PAN fibers appears rough and there seem to be some pores/holes on the fiber surface. Fig. 3A shows the SEM image of the Co_3O_4/PAN composite fibers after carbonization. The image suggests the particles are still aggregated on the surface of the fibers and are not homogeneously distributed. The inhomogeneity of the particle distribution is confirmed in Fig. 3B, which shows a higher magnification of the Co_3O_4/C composite fibers. Furthermore, the surface of the Co_3O_4/C composite fibers appear smooth with respect to the carbon fibers. A comparison of the Co_3O_4/C composite and Co_3O_4/PAN precursor fibers can be seen from Figs. 2 and 3, where the surface of the fibers has become smoother and the agglomeration of the cobalt on the surface remains the same.

Fig. 4A–E show a SEM image of the region used for collection of the electron maps and the electron mappings for carbon, cobalt, nitrogen and oxygen, respectively. The carbon map shows a homogenous distribution of carbon in the PAN fibers and indicates the absence of carbon where the cobalt particles are located, which are shown as black spots on the PAN fibers. The distribution of cobalt in the electron map confirms the non-homogenous distribution of the Co_3O_4 nanoparticles on the PAN fibers, as can be seen in Fig. 4C. The nitrogen electron map (Fig. 4D) shows the nitrogen concentration was observed to be lower in the areas where the Co_3O_4 nanomaterials are located. The lower concentration of N in the areas indicates a small correlation of the association of N in the PAN fibers with the Co_3O_4 nanoparticles. The oxygen distribution was observed to be highly correlated to the positions of the Co_3O_4 nanoparticles, as can be seen in Fig. 4E. In addition, to collect the EDS maps, EDS spectra were obtained, which show sample homogeneity from three different locations in the Co_3O_4/PAN composite fibers (Table 1). As can be seen in Table 1, the distribution of the Co_3O_4 nanoparticles does vary based on the location confirming the non-homogenous nature of the Co_3O_4/PAN composite fibers.

Fig. 5A–E shows the SEM image and EDS mappings of the Co_3O_4/C composite fibers, which were used for the electron map collection and the electron density mappings for carbon, cobalt, nitrogen and oxygen, respectively. In Fig. 5B, the carbon maps
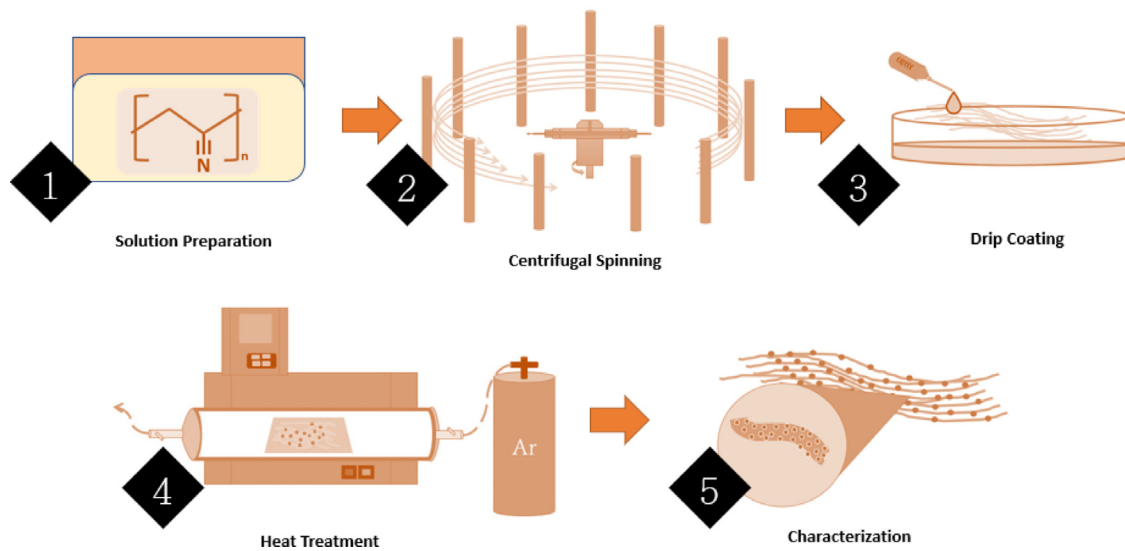
Fig. 1. Schematic showing the synthesis and processing of the Co_3O_4/C composite fibers.
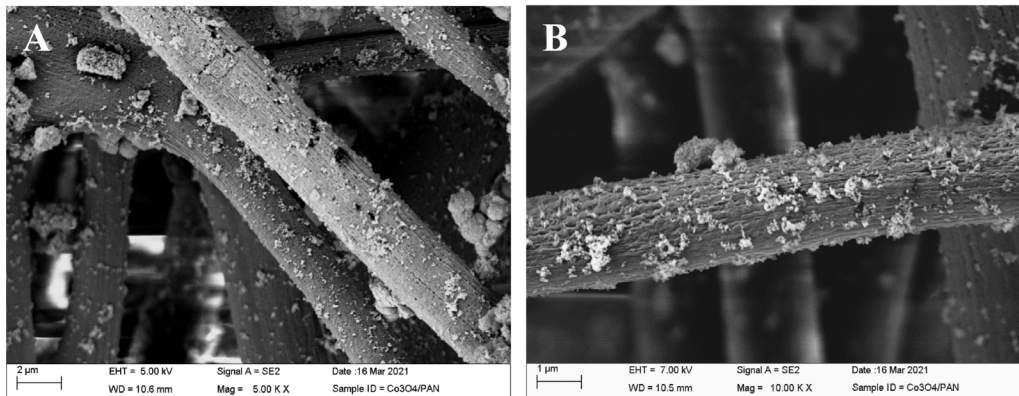
Fig. 2. SEM images of the Co_3O_4/PAN precursor fibers at 5000 X magnification (A) and at 10,000 X magnification (B).
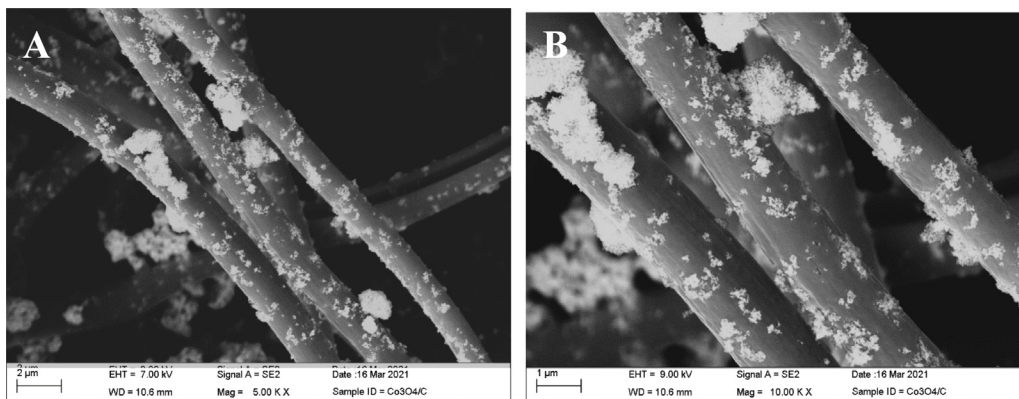
Fig. 3. SEM images of the Co_3O_4-carbon composite fibers at 5000 X magnification (A) and at 10,000 X magnification (B).

show a homogenous distribution of carbon in the Co_3O_4/C composite fibers with a few dark spots on the fibers, which correspond to the points of attachment or locations of the Co containing nanoparticles/nanoclusters. Fig. 5C shows the electron density map for Co and has several bright spots, which are representative of higher concentrations of Co. The distribution of Co in/on the fibers was observed throughout the samples; however, it is not homogenous as there are areas of high and low concentrations.

The nitrogen electron map in Fig. 5D shows a consistent and homogenous distribution of N throughout the fibers. In addition, there are no dark spots observed on the fibers, indicating that N is also associated with the cobalt in the sample. Finally, Fig. 5E shows the electron density map for oxygen, which again shows a homogenous distribution throughout the sample, with high concentrations in the areas where the cobalt is present in the sample. The higher concentration of oxygen in the areas with the
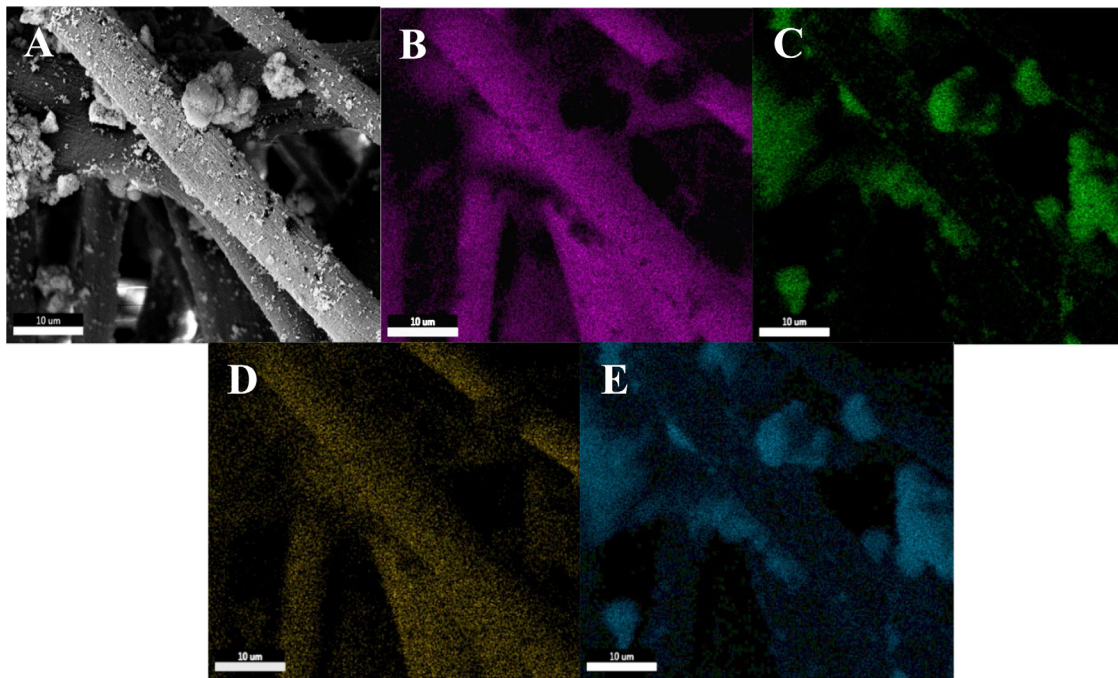
Fig. 4. SEM/EDS mapping of the Co_3O_4/PAN precursor fibers (A) SEM of the mapping area and the electron mappings for (B) carbon, (C) cobalt, (D) nitrogen and (E) oxygen.
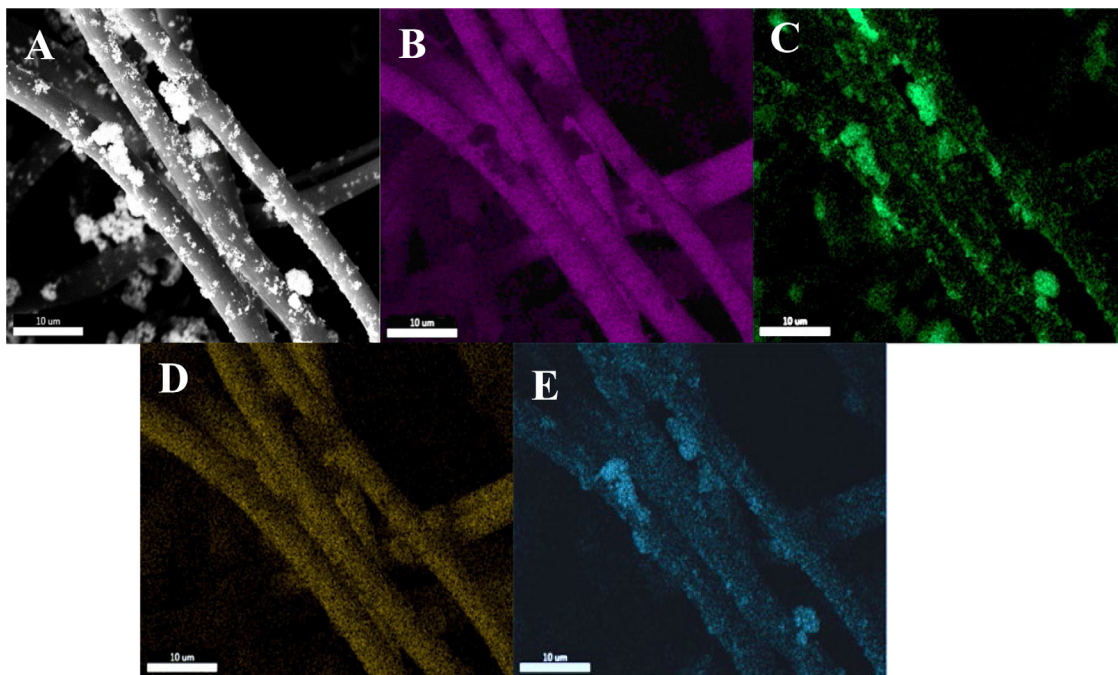
Fig. 5. SEM/EDS mapping of the Co_3O_4/C composite fibers (A) SEM of the mapping area, and the electron mappings for (B) carbon, (C) cobalt, (D) nitrogen and (E) oxygen.

cobalt may indicate that the oxygen is bound to the cobalt in the Co_3O_4/C composite fibers. In addition to the electron maps, EDS spectra were collected in three different areas in the sample. The data confirms the distribution of the cobalt in the sample does vary, as illustrated in Table 2.

3.2. BET analysis

Table 3 shows the results from the BET analysis of the samples, which included the PAN fibers, Co_3O_4/C composite fibers and the

Co_3O_4 nanoparticles (NPs). The results show that the surface area of the Co_3O_4/C composite fibers is larger than the PAN fibers. The fibers used in this work were large, which is very common for centrifugally spun fibers, as can be observed in the SEM images presented in Fig. 3(A and B). The fiber diameter was approximately 1 μm, thus a low surface area was expected. The untreated PAN fibers showed a surface area of approximately 3.1 m^2/g. The Co_3O_4 NPs showed a surface area of 25.7 m^2/g. Heat treatment of the PAN-Co_3O_4/PAN precursor fibers, used to produce the Co_3O_4/C composite material, showed an increase in surface area
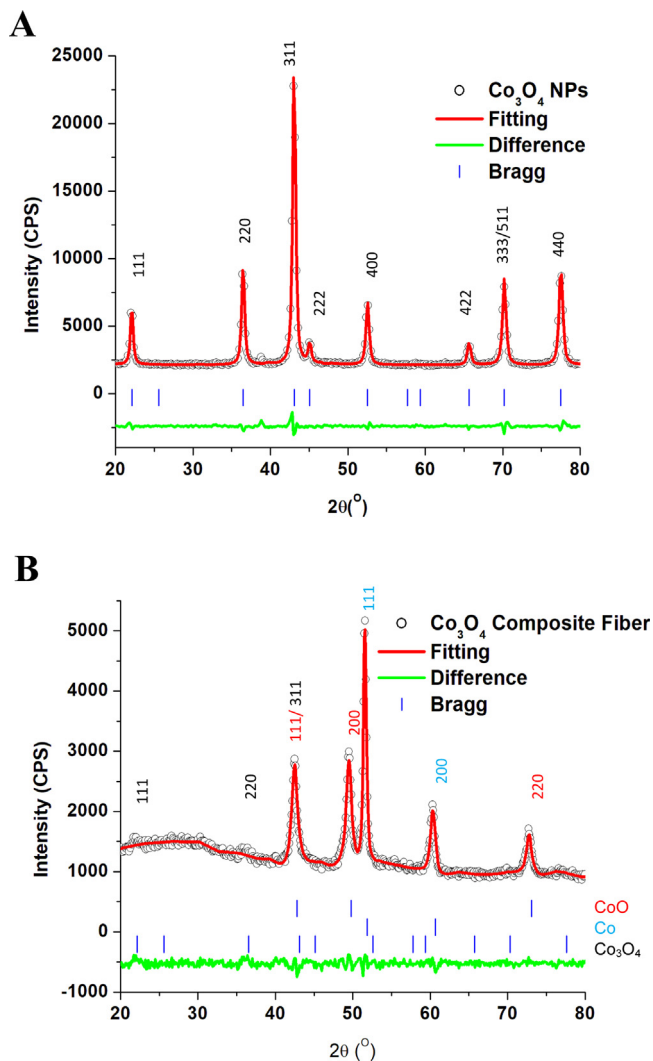
Fig. 6. (A) powder X-ray diffraction pattern of the Co_3O_4 nanoparticles used with PAN fibers for the synthesis of the Co_3O_4/C composite material. (B) X-ray powder diffraction pattern for the Co_3O_4/C composite fibers after heat treatment.. (For interpretation of the references to color in this figure legend, the reader is referred to the web version of this article.)

Table 2
EDS results for carbonized Co_3O_4/PAN composite fibers for carbon, nitrogen, cobalt and oxygen concentrations.

Element	at % Area 1	wt% Area 1	at % Area 2	wt% Area 2	at % Area 3	wt% Area 3
C	75.50	69.77	69.72	56.61	70.52	62.82
N	21.62	23.31	19.65	18.61	23.27	24.18
O	1.86	2.29	6.04	6.53	4.43	5.26
Co	1.02	4.62	4.58	18.24	1.77	7.74

from 3.072 to 5.1 m^2/g. This increase in surface area was expected due to the conversion of the PAN- to its carbon form. The surface area values are in agreement with those reported in the literature for PAN/metallic NPs composite fibers [13–15]

3.3. XRD

Fig. 6(A and B) shows the X-ray powder diffraction pattern of the Co_3O_4 NPs and the Co_3O_4/C composite fibers, prepared from the Co_3O_4/PAN precursor fibers with subsequent heat treatment. The diffraction patterns were fitted using the Le Bail fitting procedure in the Fullprof Suit of software and the crystallographic
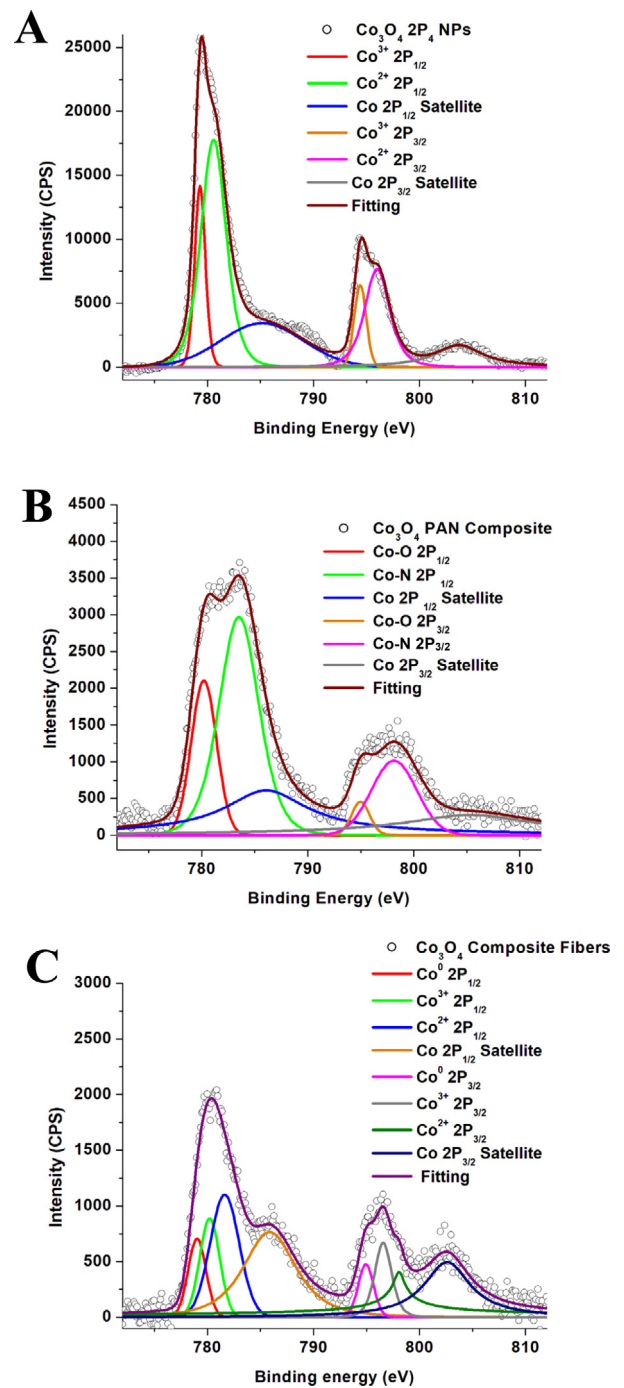
Fig. 7. The XPS spectra for (A) the Co_3O_4 nanoparticles, (B) the reaction of the Co_3O_4 nanoparticles with N in the PAN precursor fibers and (C) Co_3O_4 nanoparticles in the carbonized PAN-fibers.

Table 3
Results of BET surface area analysis of the PAN fibers, Co_3O_4/C composite fibers and the Co_3O_4 nanoparticles.

Sample	BET (m^2/g)	R^2
PAN fibers	3.072	0.999
Co_3O_4/C composite fibers	5.098	0.997
Co_3O_4 nanoparticles	25.679	0.999

data from the literature [16]. The fitting of the Co_3O_4 NPs showed the typical cubic crystal structure for the NPs, which were in the FM-3M lattice with $a = b = c = 8.021$ and all angles
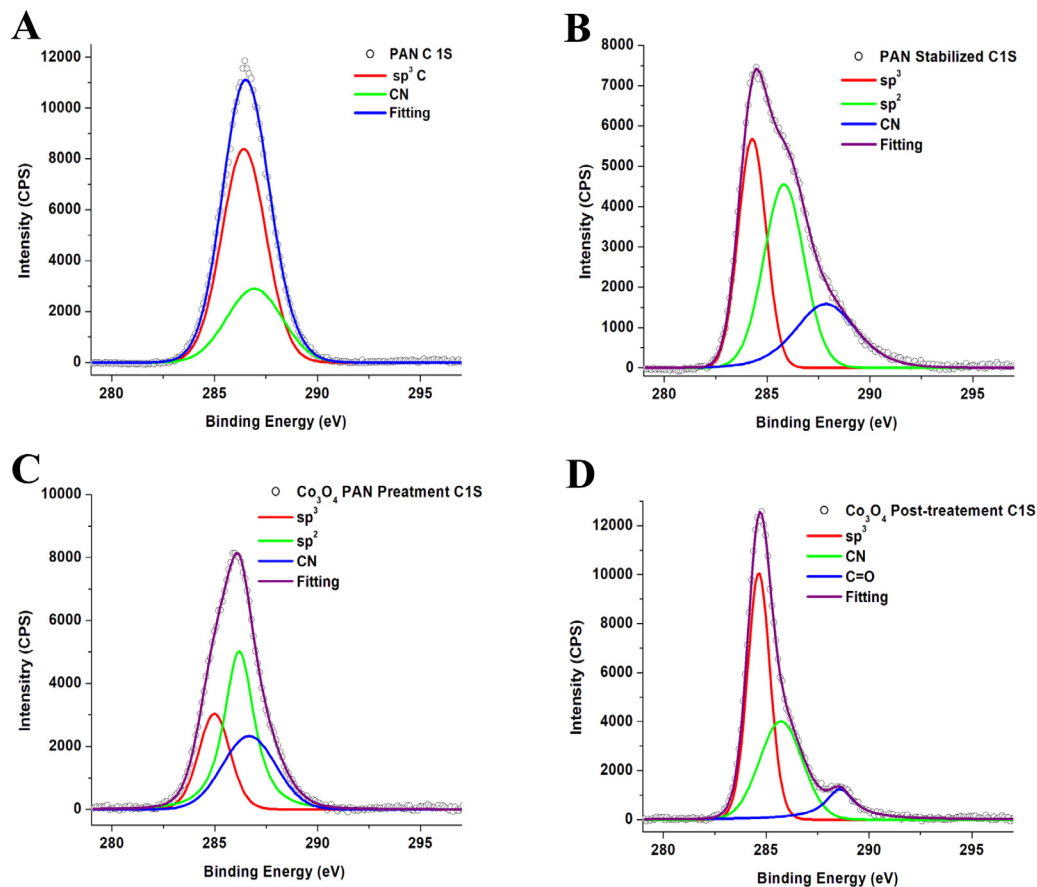
Fig. 8. C 1S XPS spectra for (A) pristine PAN fibers, (B) stabilized PAN fibers, (C) the reaction of the Co_3O_4 nanoparticles with PAN after spinning and (D) Co_3O_4 nanoparticles in the PAN fiber–matrix after carbonization.

equal to 90°. In addition, the fitting results of the Co_3O_4 NPs are in great agreement with the χ^2 value of 3.29 reported in the literature, indicating a very good fitting. The XRD results of the Co_3O_4/PAN precursor fibers after heat treatment show a completely different crystal structure. From the X-ray diffraction data, it was determined that three crystal structures were present in the sample, as can be seen in Fig. 6B. It was determined that a small portion of the sample consisted of Co_3O_4, a portion of the Co_3O_4 NPs was reduced to CoO and some of the Co_3O_4 in the sample was reduced to Co metal. The reduction of Co_3O_4 in the presence of carbon at high temperatures has been noted in the literature [17–21]. The Co-metal phase was determined to have the FM3M space group, while the Co 111 (at 51.8° in 2θ) and 220 (at 60.6° in 2θ) diffraction planes were determined to be present, denoted in light blue text in the figure. CoO was determined to be in the FM-3M space group and the CoO 111 (at 42.7° in 2θ), 200 (at 49.7° in 2θ) and 220 (at 73.0° in 2θ) diffraction planes were determined to be present; the peaks are denoted in the red text in Fig. 6. The presence of the Co_3O_4 NPs was determined to be still in the sample, however only to a small extent. The Co_3O_4 NPs were determined to be in the FM-3M crystal lattice with the Co_3O_4 diffraction planes of 111 (at 22.1° in 2θ), 220 at 36.5° and 311 at 43.1°, which are denoted in black text within the figure. The Co_3O_4 311 and the CoO 111 diffraction planes are less than $1/2$ of a degree in difference and were determined to be the same peak centered around 42.8° in 2θ. There is a good agreement between the fittings and the three phases determined in the samples, where the Le Bail fitting resulted in a χ^2 of 1.74.

3.4. XPS analysis

Fig. 7A shows the XPS pattern for the Co_3O_4 NPs. The spectrum can be divided into two regions, which are for Co $2P_{3/2}$ and Co $2P_{1/2}$. The Co $2P_{3/2}$ and Co $2P_{1/2}$ transitions are located at 779 and 795 eV, respectively. Within the Co $2P_{3/2}$ region, there were three peaks identified at 779.3, 780.5, and 785.1 eV. The peak located at 779.3 eV was determined to be the Co^{3+} $2P_{3/2}$ peak within the Co_3O_4 system, while the peak located at 780.5 eV was identified as the $Co^{2+}2P_{3/2}$ peak. The third peak located at 785.1 eV was identified as the satellite peak for the material [22–24]. Within the Co $2P_{1/2}$ region range, three peaks were identified as making up the main peaks, located at 794.3, 796.0 and 803.2 eV. The peak located at 794.3 eV was for Co^{3+}, while the Co^{2+} $2P_{1/2}$ peak was located at 796.0 eV where both peaks were consistent with the structure of Co_3O_4 NPs. The highest energy peak located at 803.2 eV was assigned as a satellite peak for the Co_3O_4-nanoparticles system. Fig. 7B shows the Co 2P spectrum for the pre-treated sample (uncarbonized PAN fibers). The Co $2P_{3/2}$ spectrum was deconvolved into three peaks, which were located at 780, 783.4 and 788.9 eV. The peak located at 788.9 eV was identified as the Co $2P_{3/2}$ satellite peak for Co, while the peak at 783.4 eV was indicative of a Co–N interaction, as was observed in the literature for cobalt bound to nitrogen in a cobalt-iron-nitride [22]. The Co–N ligation indicated a change in the chemical environment from pure Co_3O_4 nanoparticles, as shown in Fig. 7A. The binding of cobalt to the nitrogen in the PAN fibers, which in this case was determined to be acting as a cyanide ligand and complexing with the nanoparticles, generated the C–N bond observed in the sample. Finally, the peak located at 780.0 eV was linked to the presence of Co in the 2+ oxidation state bound to oxygen, as was
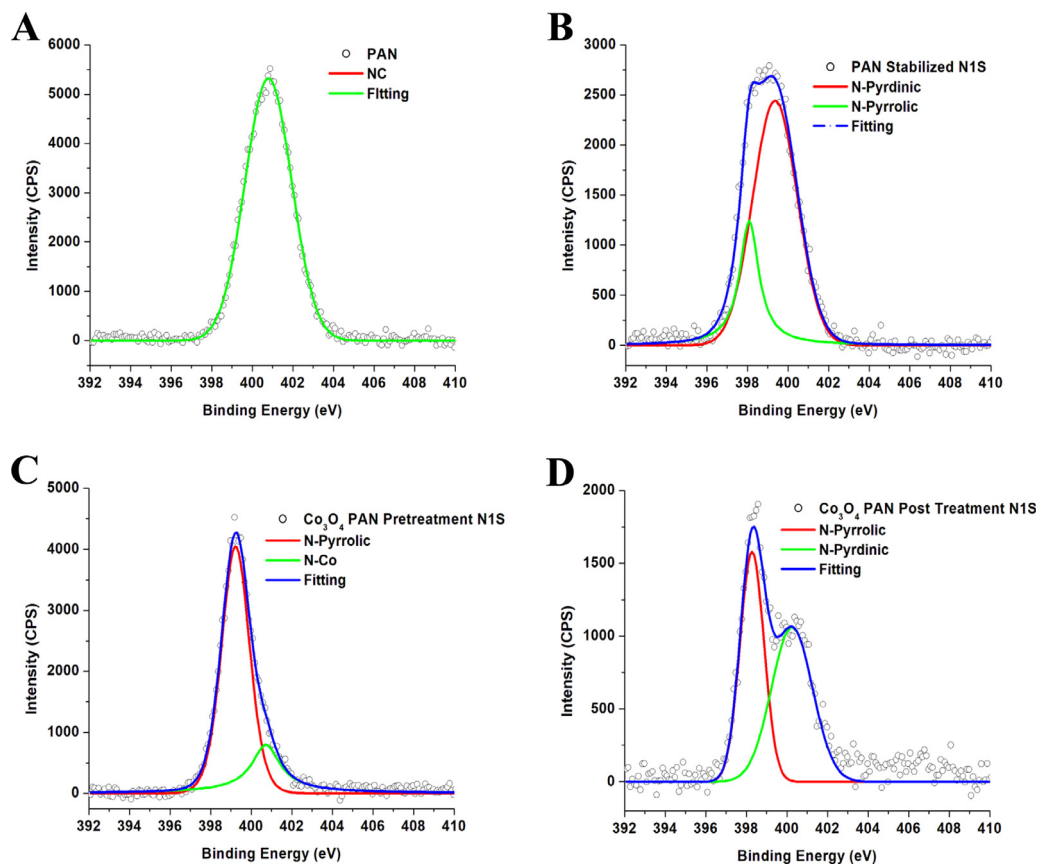
Fig. 9. N 1S XPS spectra for (A) pristine PAN, (B) stabilized PAN, (C) the reaction of the Co_3O_4 nanoparticles with PAN after spinning and (D) Co_3O_4 nanoparticles in the PAN fiber matrix after carbonization.

observed in the literature [22–24]. Similarly, the Co $2P_{1/2}$ peak can be broken down into three peaks located at 795.0, 798.2 and 806.1 eV, which represented the same chemical environments observed in the Co $2P_{3/2}$. The peak located at 806.1 eV was determined to be the satellite peak for Co 2P while those located at 798.2 and 795.0 eV were the peaks for the Co–N interaction and Co^{2+}, respectively. Fig. 7C shows the Co 2P XPS spectrum for the Co_3O_4/PAN precursor fibers after heat treatment (i.e. Co_3O_4/C composite fibers). The Co $2P_{3/2}$ peak was deconvolved into 4 different peaks located at 778.5, 799.8, 781.7 and 786.2 eV. The peak at 778.5 eV was determined to be Co metal nanoparticles due to the reduction of the Co ions, which was supported by the XRD data [24]. It should be noted that the Co metal peak position is approximately at 778 eV, with a shift of the center of approximately $\pm$ 0.6 eV [24]. The peak at 779.8 eV in the spectrum was due to the existence of some Co^{3+} in the sample, while the peak located at 781.2 eV was associated with that of Co^{2+} $2P_{3/2}$. The final peak at 786.2 eV was the Co $2P_{3/2}$ satellite peak. The satellite peak is commonly observed because of the Co–O bonding environment. Similarly, the Co $2P_{1/2}$ peak can be deconvolved into four peaks located at 794.5, 796.2, 797.8 and 802.8 eV representing Co(0), Co^{3+}, Co^{2+} and the Co–O satellite features, respectively.

The C 1S spectrum of the centrifugally spun PAN fibers is shown in Fig. 8A. This spectrum was deconvolved into two separate peaks located at 286.5 and 287 eV. The observed binding energies are typical of PAN fibers before stabilization and represent the C–C and C–N environment in the acrylonitrile structure. The peak at 286.5 eV represents the C–C binding environment, whereas the 287.0 eV represents the C≡N binding. These binding environments and binding energies have been reported in the literature [25]. The C 1S spectrum for the stabilized PAN fibers is

shown in Fig. 8B and was determined to consist of three different peaks with binding energies of 284.3, 285.9 and 288 eV. These were interpreted to be the C–C/C=C bonds in the sample, which were formed after the cyclization process of the PAN fibers. The peak centered at 285.9 eV represents C=N or C–O bonds. The addition of the Co_3O_4 nanoparticles to the PAN precursor exhibited three different chemical environments in the C 1S spectrum, as shown in Fig. 8C. The spectrum was determined to consist of three peaks located at 285.0, 286.2 and 288.6 eV, representing the C–C/C=C, C=N and C=O, binding environment, respectively [25]. The binding energies located at 286.3 and 286.8 eV were determined to be from C=O and C=N, and were shifted due to the attachment of Co through both the oxygen and nitrogen atoms. The attachment of Co to the N or O atoms would remove electron density from the associated carbon atoms and could cause the shift to the higher binding energies. The involvement of the O and N atoms in the binding of the Co is consistent with the peak-shifts observed in the Co $2P_{3/2}$ and Co $2P_{1/2}$ XPS data. The C 1S spectrum for the carbonized PAN fibers with Co_3O_4 nanoparticles is shown in Fig. 8D, which was determined to consist of three individual peaks located at 284.7, 285.8 and 288.6 eV, that are representative of the C–C/C=C, C=N–Co and C=O–Co binding environments, respectively.

Fig. 9A shows the N 1S spectrum for the pristine PAN fibers. The spectrum contains one peak centered at 400.7 eV, which is representative of the C≡N binding environment [25–27]. Fig. 9B shows the N 1S spectrum for the stabilized PAN fibers. The spectrum was determined to consist of two peaks located at 398.2 and 399.3 eV. The pyrrolic-N was observed at 399.5 eV and has a =C–N–C- binding environment, whereas the pyridinic N was located at 399.3 eV and is in a -C=N–C- binding environment [26,27]. Fig. 9C shows the N 1S spectrum for the
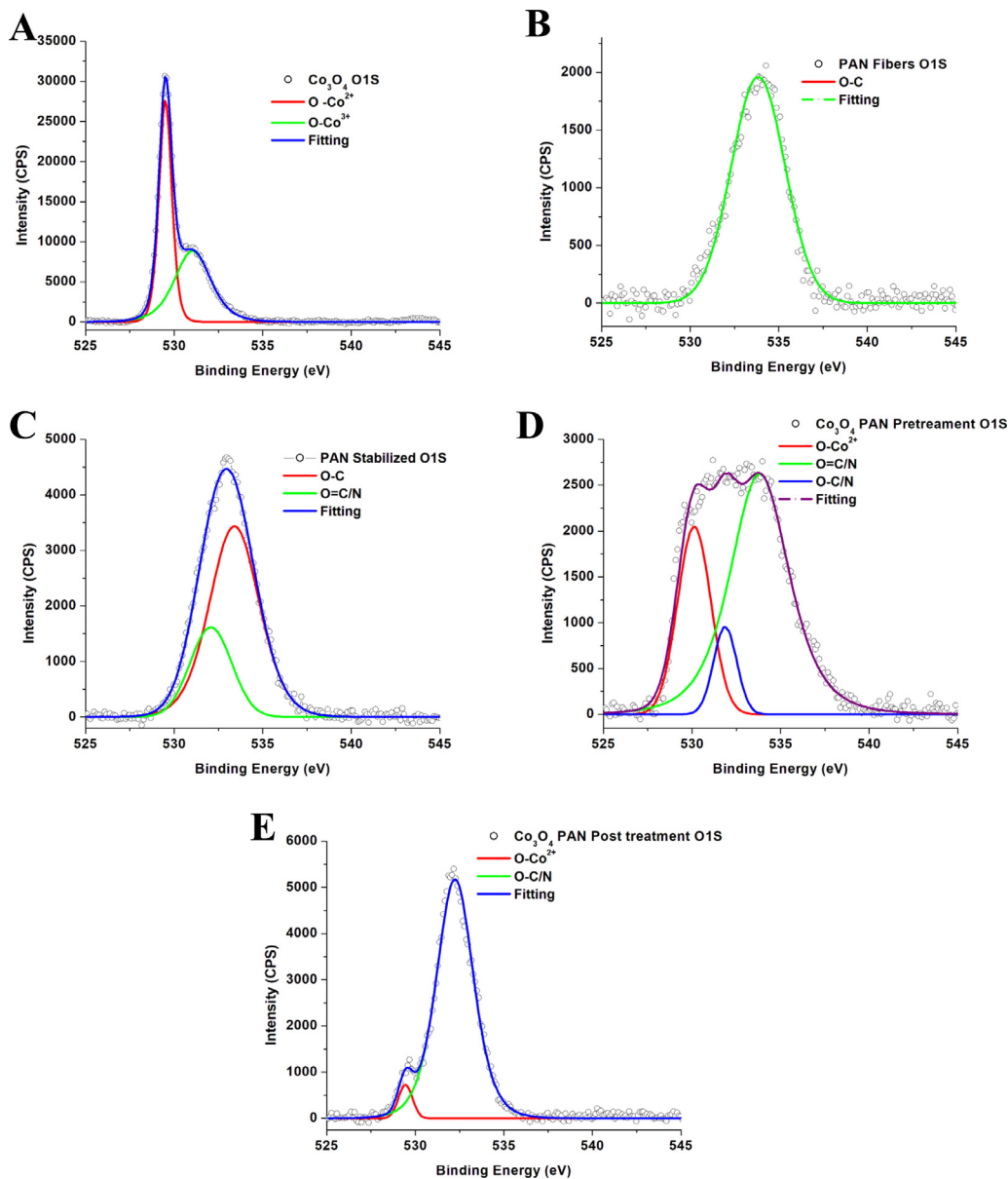
Fig. 10. O 1S XPS spectra for (A) the Co_3O_4 nanoparticles, (B) pristine PAN fibers, (C) stabilized PAN, (D) the reaction of the Co_3O_4 nanoparticles with the PAN after spinning and (E) Co_3O_4 nanoparticles in the PAN-fiber matrix after carbonization.

Co_3O_4 nanoparticles reacted with PAN before carbonization. The nitrogen was determined to have two different chemical environments located at 399.5 and 400.9 eV. The peak located at 400.9 represents the C≡N, but also represents a C=N–Co coordination environment [28]. The second peak is similar to the N-C binding environment in the PAN after stabilization and the production of the pyridinic peak at 399.5 eV indicates ring formation in the structure. This formation of a ring in the structure appears to be induced by the presence of the cobalt oxide nanoparticles, causing a change in the nitrogen electron environment and ring formation. An interaction was observed between Co and nitrogen in the structure, causing a reduction in the Co, which supported the XRD results and the Co $2P_{3/2}$ and Co $2P_{1/2}$ XPS data. Fig. 9D shows the XPS spectrum of the Co_3O_4 nanoparticles in PAN fibers after carbonization, which indicates the presence of two nitrogen environments, pyrrolic and pyridinic. These two peaks, located at 398.3 and 399.3 eV, are commonly observed in PAN fibers after stabilization and carbonization.

Fig. 10A shows the O 1S spectrum for the Co_3O_4 nanoparticles, determined to consist of two separate binding environments

which were located at 531.2 and 529.6 eV. These peaks are commonly observed in Co_3O_4 and represent the Co^{3+}–O and Co^{2+}–O binding environments [28]. Fig. 10B shows the O 1S spectrum for the PAN fibers, which was determined to have a low intensity peak located at 533.5 eV, indicative of an O–C bond, indicating modest oxidation of the PAN fibers [27]. Fig. 10C shows the O1S spectrum after stabilization, with a C–O peak present at 533.5 eV. The stabilized PAN fibers also show a secondary peak located at 532.1 eV, indicating the presence of oxygen in the –1 oxidation state, likely bound to a nitrogen atom. Fig. 10D shows the Co_3O_4/PAN-precursor fibers, with oxygen being present in three different binding environments. The first, located at 533.5 eV, is related to the formation of C–O bonds in the samples. The others are related to the Co^{2+}–O and C=O binding environments, which are located at 530 and 531.8 eV, respectively. Fig. 10E shows the oxygen binding environment after carbonization. The oxygen binding environment after carbonization results in a small peak at approximately 529 eV and second peak centered around 533 eV, which correspond to Co–O and the C–O/C=O binding environments.

4. Conclusion

The synthesis of Co_3O_4/carbon fibers was observed through the addition of Co_3O_4 to PAN fibers, followed by thermal treatment. SEM analysis showed that the fibers consisted of areas of high and low concentrations of Co, while the EDS mapping indicated a correlation between Co and N and Co–O. The BET results showed that the surface area of the PAN fibers was low, but did increase after coating Co_3O_4 NPs on the PAN fibers and subsequent heat treatment (i.e. heating and stabilization in air) and carbonization. The surface area of the Co_3O_4/C composite fibers was approximately double that of the PAN fibers. The characterization results by EDS, XRD and XPS confirmed that the Co_3O_4/C composite sample was composed of CoO, Co, Co_3O_4 and carbon, with the Co_3O_4 NPs being a minor fraction in the samples. The reduction of Co_3O_4 to form CoO and Co metal has been previously reported. The synthesis method reported in this work is considered as a simple and rapid technique for the development of CoO/Co metal composite carbon fibers, which have the potential to be used as anodes in LIBs and in catalysis.

CRediT authorship contribution statement

J. Ayala: Investigation, Writing – first draft. **D. Ramirez:** Investigation. **E. Fletes:** Investigation. **H. Morales:** Writing – review & editing. **J.G. Parsons:** Formal analysis, Visualization, Writing – review & editing, Final draft. **M. Alcoutlabi:** Writing – review & editing, Supervision, Funding, Conceptualization, Administration.

Declaration of competing interest

The authors declare that they have no known competing financial interests or personal relationships that could have appeared to influence the work reported in this paper.

Acknowledgments

References

[1] L. Zuniga, G. Gonzalez, R.O. Chavez, J.C. Myers, T.P. Lodge, M. Alcoutlabi, Centrifugally spun α-Fe$_2$O$_3$/TiO$_2$/carbon composite fibers as anode materials for lithium-ion batteries, Appl. Sci.-Basel 9 (19) (2019) 4032, http://dx.doi.org/10.3390/app9194032.

[2] M.D. Calisir, A. Kilic, Mater. Lett., A comparative study on SiO$_2$ nanofiber production via two novel non-electrospinning methods: Centrifugal spinning vs solution blowing, Mater. Lett. 258 (2020) 126751, http://dx.doi.org/10.1016/j.matlet.2019.126751.

[3] Y. Yan, K. Bao, T. Liu. J. Cao, J. Feng, J. Qi, Minutes periodic wet chemistry engineering to turn bulk Co-Ni foam into hydroxide based nanosheets for efficient water decomposition, Chem. Eng. J. 401 (2020) 126092.

[4] Y. Yan, J. Lin, J. Cao, S. Guo, X. Zheng, J. Feng, J. Qi, Junlei, Activating and optimizing the activity of NiCoP nanosheets for electrocatalytic alkaline water splitting through the V doping effect enhanced by P vacancies, J. Mater. Chem. A 7 (2019) 24486–24492.

[5] V. Lukasova, M. Buzgo, K. Vocetkova, V. Sovkova, M. Doupnik, E. Himawan, A. Staffa, R. Sedlacek, H. Chlup, F. Rustichelli, E. Amler, M. Rampichova, Needleless electrospun and centrifugal spun poly-ε-caprolactone scaffolds as a carrier for platelets in tissue engineering applications: A comparative study with hMSCs, Mater. Sci. Eng. C Mater. Biol. Appl. 97 (2019) 567–575, http://dx.doi.org/10.1016/j.msec.2018.12.069.

[6] L. Cremar, J. Gutierrez, J. Martinez, L.A. Materon, R. Gilkerson, F.H. Xu, K. Lozano, Development of antimicrobial chitosan based nanofiber dressings for wound healing applications, Nanomed. J. 5 (2018) 6–14.

[7] D. De la Garza, F. De Santiago, L. Materon, M. Chipara, M. Alcoutlabi, Fabrication and characterization of centrifugally spun poly(acrylic acid) nanofibers, J. Appl. Polym. Sci. 136 (2019) http://dx.doi.org/10.1002/app.47480.

[8] L. Ji, O. Toprakci, M. Alcoutlabi, Y. Yao, Y. Li, S. Zhang, B. Guo, Z. Lin, X. Zhang, α-Fe$_2$O$_3$ Nanoparticle-loaded carbon nanofibers as stable and high-capacity anodes for rechargeable lithium-ion batteries, ACS Appl. Mater. Interfaces 4 (2012) 2672–2679, http://dx.doi.org/10.1021/am300333s.

[9] N. Wongittharom, C.H. Wang, Y.C. Wang, G.T.K. Fey, H.Y. Li, T.Y. Wu, T.C. Lee, J.K. Chang, Charge-storage performance of Li/LiFePO$_4$ cells with additive-incorporated ionic liquid electrolytes at various temperatures, J. Power Sources 260 (2014) 268–275.

[10] T. Yoon, C. Chae, Y.-K. Sun, X. Zhao, H.H. Kung, J.K. Lee, Bottom-up in situ formation of Fe$_3$O$_4$ nanocrystals in a porous carbon foam for lithium-ion battery anodes, J. Mater. Chem. 21 (2011) 17325–17330.

[11] M. Akia, N. Salinas, S. Luna, E. Medina, A. Valdez, J. Lopez, J. Ayala, M. Alcoutlabi, K. Lozano, In situ synthesis of Fe$_3$O$_4$-reinforced carbon fiber composites as anodes in lithium-ion batteries, J. Mater. Sci. 54 (2019) 13479–13490.

[12] H.M. Golecki, H. Yuan, C. Glavin, B. Potter, M.R. Badrossamay, J.A. Goss, M.D. Phillips, K.K. Parker, Effect of solvent evaporation on fiber morphology in rotary jet spinning, Langmuir 30 (2014) 13369–13374.

[13] N. Kaerkitcha, S. Chuangchote, T. Sagawa, Control of physical properties of carbon nanofibers obtained from coaxial electrospinning of PMMA and PAN with adjustable inner/outer nozzle-ends, Nanoscale Res. Lett. 11 (2016) 186, http://dx.doi.org/10.1186/s11671-016-1416-7.

[14] S.H. Park, B.C. Kim, S.M. Jo, D.Y. Kim, W.S. Lee, Cabon nanofibrous materials prepared from electrospun polyacrylonitrile nanofibers for hydrogen storage, MRS Proc. 837 (2004) N3.14, http://dx.doi.org/10.1557/PROC-837-N3.14.

[15] S. Yarova, D. Jones, F. Jaouen, S. Cavaliere, Strategies to hierarchical porosity in carbon nanofiber webs for electrochemical applications, Surf. 2 (2019) 159–176.

[16] J. Rodriguez-Carvajal, Recent advances in magnetic structure determination by neutron powder diffraction, Phys. B 192 (1993) 55–69.

[17] S. Yao, R. Guo, F. Xie, Z. Wu, K. Gao, C. Zhang, X. Shen, T. Li, S. Qin, Electrospun three-dimensional cobalt decorated nitrogen doped carbon nanofibers network as freestanding electrode for lithium/sulfur batteries, Electrochim. Acta 337 (2020) 135765.

[18] N. Cai, M. Chen, M. Liu, J. Wang, L. Shen, J. Wang, X. Feng, F. Yu, Meso-microporous carbon nanofibers with in-situ embedded co nanoparticles for catalytic oxidization of azo dyes, J. Mol. Liq. 289 (2019) 111060.

[19] S. Sasaki, K. Fujino, Y. Takéuchi, X-ray determination of electron-density distributions in oxides, MgO, MnO, CoO, and NiO, and atomic scattering factors of their constituent atoms, Proc. Jpn. Acad. Ser. B 55 (2) (1979) 43–48.

[20] R. Fruchart, A. Roger, J. Senateur, Crystallographic and magnetic properties of solid solutions of the phosphides M_2P, M = Cr, Mn, Fe, Co, and Ni, J. Appl. Phys. 40 (1969) 1250–1257.

[21] S. Pindar, N. Dhawan, Carbothermal reduction of spent mobile phones batteries for the recovery of lithium, cobalt, and manganese values, JOM 71 (2019) 4483–4491, http://dx.doi.org/10.1007/s11837-019-03799-9.

[22] Y. Wang, D. Liu, Z. Liu, C. Xie, J. Huo, S. Wang, Porous cobalt–iron nitride nanowires as excellent bifunctional electrocatalysts for overall water splitting, Chem. Commun. 52 (2016) 12614–12617.

[23] M. Madkour, Y.K. Abdel-Monem, F. Al Sagheer, Controlled synthesis of NiO and Co$_3$O$_4$ nanoparticles from different coordinated precursors: Impact of precursor's geometry on the nanoparticles characteristics, Ind. Eng. Chem. Res. 55 (2016) 12733–12741.

[24] M. Domínguez, E. Taboada, H. Idriss, E. Molins, J. Llorca, Fast and efficient hydrogen generation catalyzed by cobalt talc nanolayers dispersed in silica aerogel, J. Mater. Chem. 20 (2010) 4875–4883.

[25] G.Y. Baek, H.S. Lee, J.-M. Jung, I.-T. Hwang, J. Shin, C.-H. Jung, J.-H. Choi, Preparation of conductive carbon films from polyacrylonitrile/graphene oxide composite films by thermal treatment, J. Ind. Eng. Chem. 58 (2018) 87–91.

[26] M. Kim, D.-H. Nam, H.-Y. Park, C. Kwon, K. Eom, S. Yoo, J. Jang, H.-J. Kim, E. Cho, H. Kwon, Cobalt-carbon nanofibers as an efficient support-free catalyst for oxygen reduction reaction with a systematic study of active site formation, J. Mater. Chem. A 3 (2015) 14284–14290.

[27] B. Pollack, S. Holmberg, D. George, I. Tran, M. Madou, M. Ghazinejad, Nitrogen-rich polyacrylonitrile-based graphitic carbons for hydrogen peroxide sensing, Sensors 17 (2017) 2407.

[28] K. Artyushkova, Misconceptions in interpretation of nitrogen chemistry from X-ray photoelectron spectra, J. Vac. Sci. Technol. A 38 (2020) 031002.